Phase Diagrams of Stoichiometric Polyelectrolyte−Surfactant Complexes

Michael J. Leonard and Helmut H. Strey*

Department of Polymer Science and Engineering, Box 34530, University of Massachusetts, Amherst, Massachusetts 01003

Received March 19, 2003; Revised Manuscript Received October 10, 2003

ABSTRACT: Phase diagrams for a series of self-assembled, stoichiometric poly[(acrylate)-*co*-acrylamide]−cetyltrimethylammonium (PAAm−CTA^+) complexes in aqueous environments have been established using small-angle X-ray scattering (SAXS). Space groups and unit cell dimensions for each observed structure were measured as a function of salt type, ionic strength, polyelectrolyte charge density, and applied osmotic pressure. As osmotic pressure and charge density were increased, a phase sequence of $Pm3n$ cubic ↔ hexagonally close-packed cylinders (hcpc) ↔ lamellar was observed over an osmotic pressure range of 0−1000 atm. This progression of structures was accompanied by a concomitant reduction in the Bragg spacings within each phase, and the osmotic pressure dependence of these spacings indicated the presence of exponential forces between surfactant assemblies. Typical unit cell sizes were on the order of 100−150 Å for the cubic phase, 45−60 Å for the hexagonal phase, and 25−35 Å for the lamellar phase. Bragg spacings were also found to increase as ionic strength increased for each salt type studied, indicating that counterion release is a major driving force in the assembly of polyelectrolyte−surfactant complexes. At 1 M ionic strength, the complexes tended to dissociate into less well-ordered structures, presumably due to their becoming nonstoichiometric.

Introduction

Interaction between macroions of opposite charge is a recurring concept in biological self-assembly.[1] Examples include complexation of DNA with histone proteins inside cell nuclei,[2] protamine-induced DNA condensation inside sperm heads,[3−5] and the formation of arterial plaque—a complex between positively charged low-density lipoprotein and negatively charged polysaccharides.[6,7] Throughout the past several decades, researchers have recognized the potential of electrostatically driven self-assembly as a facile structure-forming tool, and significant efforts have been made to elucidate assembly mechanisms as well as to characterize the wide variety of observed structures. Complexes between polyelectrolytes and oppositely charged, small-molecule surfactants provide especially good examples of electrostatic self-assembly and, as such, have attracted a significant amount of attention, both theoretically[8−11] and experimentally.[12−17] Complexes formed between flexible, highly charged polyelectrolytes and oppositely charged surfactants at stoichiometric charge ratios have been of particular experimental interest, since they often form water-insoluble complexes possessing long-range nanoscopic order.[18−25]

While purely electrostatic interactions undoubtedly play a role during complexation, counterion release is believed to be the major driving force for the self-assembly process in these and other highly charged systems.[26−28] Prior to complexation, the polyelectrolyte and surfactant counterions are restricted to regions close to the surfaces of both the surfactant micelles and the polyelectrolyte chains, a phenomenon known as Manning condensation.[29] Upon adsorption of a polyelectrolyte chain to the surface of the ionic surfactant micelle, the counterions bound to both species are released into the bulk solution, which gives rise to a significant increase in the overall entropy of the system. Other possible contributions to the free energy include the conformational entropy of the polyelectrolyte, the elastic energy of the surfactant surface, and hydrophobic and steric interactions between the polyelectrolyte chain and the surfactant. The combination of these driving forces makes polyelectrolyte−surfactant binding significantly more favorable than micelle formation. This point is evidenced by the fact that, in the presence of polyelectrolytes, critical aggregation concentrations (cac) of surfactants in dilute solution tend to be orders of magnitude lower than critical micelle concentrations (cmc).[30,31]

Polyelectrolyte−surfactant complexation has been known for quite some time, and many studies have been devoted to characterizing the phase behavior of these systems. Previous work concerning stoichiometric complexes involved the study of morphological changes under various conditions, such as the variation of polymer charge density,[21,32,33] surfactant tail length,[19,34−36] and temperature.[36] Frequently, such studies involved the exposure of cross-linked polyelectrolyte gels to low concentrations (below cmc) of aqueous surfactant.[19,33,37] Other studies have considered polyelectrolyte−surfactant complex structure at varying surfactant concentrations[17,22,38] and water contents.[38,39] Often in such work, the stoichiometric complex represented one of several concentration regimes. In this paper, we report our effort to establish a comprehensive phase diagram of stoichiometric polyelectrolyte−surfactant complexes by studying the thermodynamics and structure of a single model system of fixed composition while manipulating several environmental variables. Specifically, our model system consisted of a series of poly[(acrylate)-*co*-acrylamide]−cetyltrimethylammonium (PAAm−CTA^+) complexes whose phase behavior was monitored as a function of ionic strength, salt type,

* Corresponding author: e-mail strey@mail.pse.umass.edu; phone (413) 577-1317; Fax (413) 545-0082.

10.1021/ma034352c CCC: $25.00
Published on Web 11/20/2003

osmotic pressure, and linear polyelectrolyte charge density.

Experimental Section

Materials. Poly(sodium acrylate) (PSA, Aldrich, $\bar{M}_N$ = 30 000 g mol^{-1}, 40 wt % aqueous solution), poly[(sodium acrylate)-*co*-acrylamide] (PSAAm, Polysciences, 70%, 40%, and 10% carboxylate contents, $\bar{M}_N$ = 200 000, 10 000 000, and 200 000 g mol^{-1}, respectively), sodium chloride (Mallinckrodt), sodium bromide (Aldrich), cetyltrimethylammonium chloride (CTACl, Aldrich, 1.04 M aqueous solution), poly(ethylene glycol) (PEG, Fluka, $\bar{M}_N$ = 8000 g mol^{-1}), and ethylenediaminetetraacetic acid (EDTA, Sigma molecular biology grade) were used as received. Tris(hydroxymethylaminomethane) (TRIS base, Sigma molecular biology grade) was adjusted to pH 7.0 (HCl) before use. All materials were used as received without further purification.

Methods. *Polyelectrolyte Solutions.* Concentrated solutions of PSA were prepared in 10 mM, 100 mM, and 1 M solutions of NaCl and NaBr which were buffered in a mixture of 10 mM TRIS base/1 mM EDTA (10-1 TE). The 70%, 40%, and 10% carboxylate content polyelectrolyte solutions were prepared at concentrations of 5, 1, and 5 wt %, respectively, by combining the vacuum-dried polyelectrolyte powders with each of the salt solutions just mentioned.

Complex Preparation and Osmotic Stress Experiments. Polyelectrolyte−surfactant complexes were prepared by combining CTACl solution with a stoichiometric amount (based on charge) of concentrated polyelectrolyte solution, followed by vigorous mixing. Immediately upon the addition of approximately 10 mL water to these mixtures, a solid white precipitate formed. The precipitate was isolated by centrifugation, washed with three 50 mL aliquots of water to remove excess ions, and was allowed to air-dry for approximately 8 h. Pieces of the dried complexes were then placed in large reservoirs of aqueous sodium bromide and sodium chloride solutions (10 mM, 100 mM, and 1 M) with PEG concentrations in each solution ranging from 0 to 50 wt %, corresponding to a calculated osmotic pressure range of 0−110 atm at 25 °C. Previous work[40−42] describes the experimentally determined relationship between PEG 8000 concentration and osmotic pressure. Each of these solutions was buffered in 10-1 TE (pH 7). The samples were then allowed to equilibrate with their respective stressing solutions for 1 month at room temperature. During this time, samples were periodically vortexed to ensure PEG solution homogeneity. Cetyltrimethylammonium bromide (CTABr) was generated in situ by exchange of the CTACl chloride ion with the free bromide ions in the NaBr−PEG solutions. To access osmotic pressures greater than those solution stress could provide, pieces of dehydrated 40%, 70%, and 100% charge complexes were sealed in separate polyethylene chambers containing saturated NaBr, CH_3CO_2Na, and KCl solutions, having relative humidities of 57%, 77%, and 89%, respectively[43] (approximate corresponding osmotic pressures were 200, 450, and 1000 atm, respectively). Samples were suspended above each saturated salt solution on a small platform inside the sealed chambers, and the complexes were allowed to equilibrate in this fashion for 1 month. It is important to note that no salt was added to these complexes either before or after equilibration.

Measurements. Small-angle X-ray scattering (SAXS) measurements were performed using a Rigaku RU-H3R rotating anode X-ray diffractometer (operating at 1.2 kW, equipped with a multilayer focusing optic: point focus (100 μm)^2; Osmic Inc., type CMF23-46Cu8) and a home-built evacuated Statton-type scattering camera. The sample cells used for the solution osmotic stress measurements consisted of Teflon cards sandwiched between thin Mylar windows which allowed the solid samples to remain in equilibrium with the stressing solutions during the measurements while isolating the samples from vacuum. For the complexes equilibrated against saturated salt vapor, a Mylar-windowed sample cell consisting of two connected chambers was used, which allowed the sample to remain in a saturated salt vapor environment during the X-ray measurements. The sample-to-detector distance was 460 mm, which corresponds to a q range of 0.0698 Å$^{-1} \leq q \leq$ 0.625 Å^{-1} with $q = (4\pi/\lambda)\sin(\theta/2)$, where θ is twice the Bragg angle, and the incident beam wavelength was 1.54 Å, corresponding to 8 keV Cu Kα radiation. Scattering patterns were acquired with 10 cm × 15 cm Fuji ST-VA image plates in conjunction with a Fuji BAS-2500 image plate scanner. The X-ray scattering intensity profiles were obtained from radial averages of the scattering pattern intensities, using procedures developed by our research group for the Igor Pro software package (Wavemetrics, Inc., Lake Oswego, OR).

Results and Discussion

The Osmotic Stress Method: General Comments. The osmotic stress method provides a means to investigate the microscopic and thermodynamic details of intermolecular interactions and has been successfully employed to measure intermolecular forces in lamellar stacks of lipid bilayers[44,45] and in hexagonal arrays of semistiff biopolymers, such as DNA,[4,5,46] collagen,[47] and various polysaccharides.[48,49] The essence of the method involves the controlled removal of water from samples in aqueous environments via the application of osmotic pressure from an inert species present in solution. The thermodynamic work required to remove water from the sample is equivalent to the work required to push the constituent molecules closer together. Experimentally, samples are equilibrated against a large excess of polymer solution whose osmotic pressure is known as a function of concentration, either through a dialysis membrane or across the solid−liquid phase boundary in phase-separated samples. Neutral and highly water-soluble polymers, such as PEG and dextran, are well suited for use as osmotic stressing agents. For most charged biopolymer systems, higher molecular weight PEG is excluded from the interior of the sample as long as its radius of gyration is larger than the average distance between two polymer chains inside the sample. Under such conditions, osmotic pressures in excess of 300 atm can be achieved, and sample densities can be determined by X-ray scattering measurements of intermolecular distances.

Using polymer solutions to apply osmotic stress has several advantages over the water vapor pressure method. While the osmotic pressure is set by the polymer concentration in the stressing solution, the salt activity can be fixed independently by adding salt to this solution. Since all activities are controlled by the stressing solution, the phase of the sample will thus be precisely specified—there can be no phase coexistence as long as the system under study remains isolated from the stressing solution. The osmotic stress method also provides information about the free energy of the system, which can be obtained by integrating the equation of state.[50]

General Phase Sequence. Most of the stoichiometric polyelectrolyte−surfactant complexes considered for this study exhibited both high and low degrees of nanoscopic order, depending on the experimental conditions chosen. For those complexes that were well-ordered, we observed the following general sequence of structures as a function of decreasing water content: $Pm3n$ cubic ↔ hexagonally close-packed cylinders (hcpc) ↔ lamellar. Representative SAXS patterns obtained for each of these structures during this study are shown in Figure 1. The ratios between the peak positions follow the characteristic patterns for each structure: $\sqrt{2}$, $\sqrt{4}$, $\sqrt{5}$, $\sqrt{6}$, $\sqrt{8}$, $\sqrt{10}$, $\sqrt{12}$, $\sqrt{14}$, for $Pm3n$; 1, $\sqrt{3}$, $\sqrt{4}$, $\sqrt{7}$,

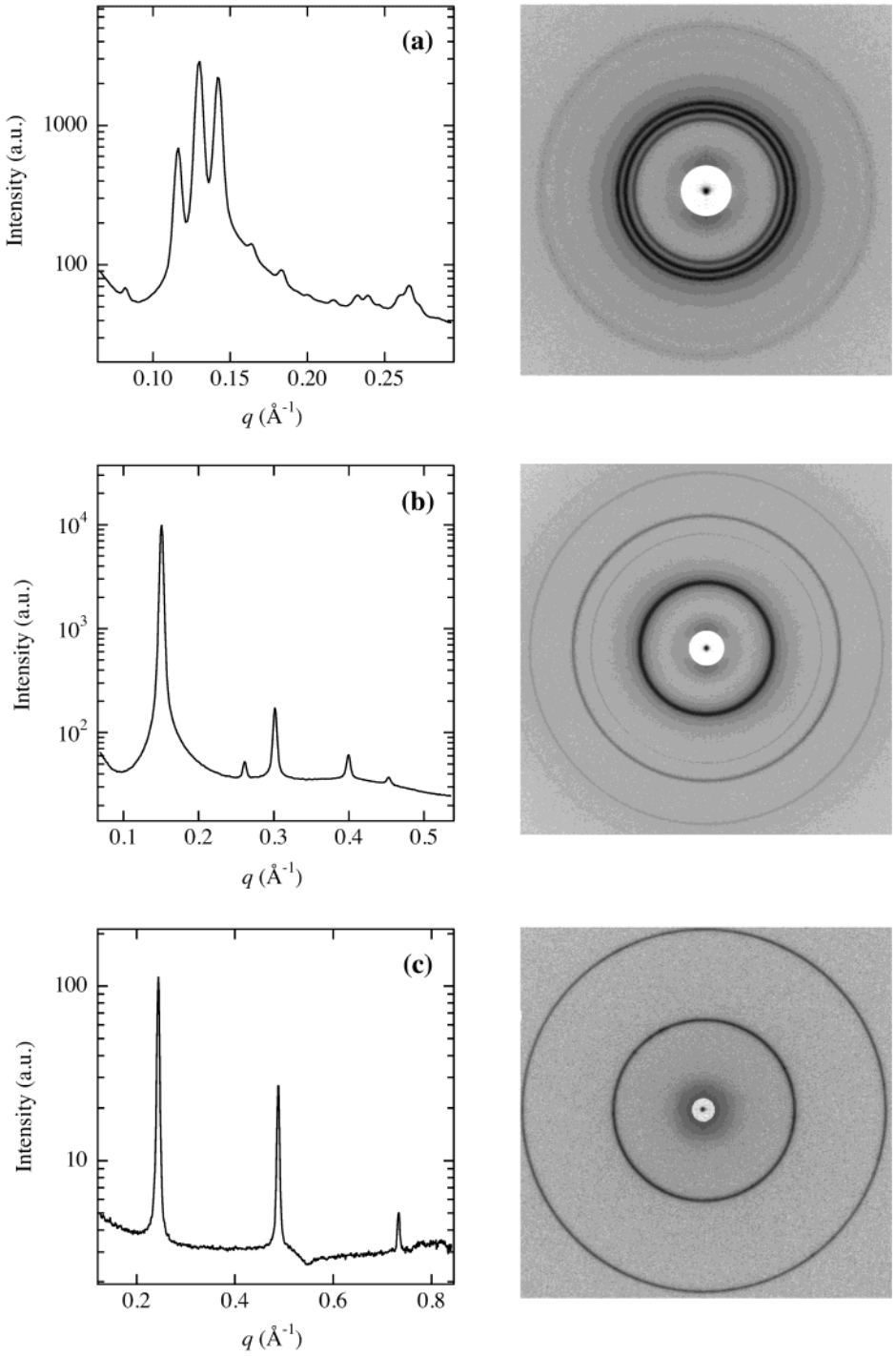

Figure 1. SAXS patterns and angular-averaged scattering profiles for 100% charge PAAm−CTA^+ complexes in (a) 10 mM NaCl, (b) 50% PEG solution in 10 mM NaCl, and (c) saturated NaBr vapor (57% relative humidity). The peak positions correspond to *Pm*3*n* cubic, hcpc, and lamellar unit cell structures, respectively, and are representative of the types of patterns obtained from other complexes considered for this study.

$\sqrt{9}$, for hcpc; 1, 2, 3 for lamellar. Note that the (110) diffraction signal is the first observable peak in the scattering profile for *Pm*3*n* cubic structure. This particular sequence is brought about by the competition of spontaneous curvature and molecular packing constraints and has been previously observed in polyacrylate−CTA^+ complexes with varying surfactant and water contents.[38] Interestingly, this sequence is also followed by aqueous cetyltrimethylammonium acetate as a function of increasing concentration.[17]

In contrast to the phase sequence observed here, the sequence of structures in aqueous bromide surfactant systems tends to follow a slightly different sequence: micellar ↔ hexagonal (spheres or cylinders) ↔ orthorhombic ↔ lamellar as a function of increasing amphiphile concentration.[17,51,52] The absence of the *Pm*3*n* structure in this sequence is due to the specific effect of the bromide ion, which tends to promote the formation of elongated micelles over structures possessing higher degrees of curvature.[17]

The occurrence of a *Pm*3*n* cubic phase represents an important morphological difference between bromide surfactant systems and the polyelectrolyte−surfactant systems studied here. This phase, which is also known

Table 1. Unit Cell Sizes for PAAm−CTA$^+$ in 100 mM NaBr[a]

charge density (%)	structure	Π_i (atm)	Π_f (atm)	a_i (Å)	a_f (Å)
100	hcpc	0	110	52.0	50.9
70	*Pm*3*n*	0	50	118.3	116.9
40	*Pm*3*n*	20	110	131.2	117.5

[a] Π_i = lowest osmotic pressure where structure was observed, Π_f = highest osmotic pressure where structure was observed, a_i = unit cell parameter a at Π_i, and a_f = unit cell parameter a at Π_f. Unit cell sizes for the hcpc phase were calculated from the following equation: $1/d^2 = \sqrt{3}a/[2(h^2 + hk + k^2)^{1/2}]$, where (100) = ($hk$0). Unit cell sizes for the *Pm*3*n* phase were calculated from the following equation: $1/d^2 = (h^2 + k^2 + l^2)^{1/2}/a^2$, where (210) = ($hkl$).

as the A15 lattice and the β tungsten lattice, has been observed frequently in similar hard core/soft corona colloidal systems.[17,33,53] Its existence has been addressed theoretically by Kamien and co-workers,[54] who used a modified hard-core/soft-shell potential to model its evolution from close-packed cubic structures. The *Pm*3*n* phase is believed to arise from frustration between the hard-core excluded-volume interaction and the surface interaction due to overlapping soft coronas and, as such, illustrates the so-called "close packing vs minimal area" principle. In our case, polyelectrolyte chains surrounding the surfactant micelles comprise the soft shell.

Phase Behavior in 10 and 100 mM Salt. *Osmotic Stress Effects*. Osmotic pressure vs Bragg distance curves were constructed from SAXS data obtained from the complexes bathed in PEG solutions containing either sodium bromide or sodium chloride. These results are shown in Figures 2 and 3, respectively, where the positions of the (100) peaks of the hcpc phase and the (210) peaks of the *Pm*3*n* phase have been plotted. Each of the curves indicates an exponential relationship between osmotic pressure and distance, where increased osmotic pressure brought about a reduction in Bragg spacing. Table 1 shows the range of unit cell sizes obtained in 100 mM bromide, as an example. This exponential relationship has frequently been observed in osmotic stress experiments[46,48,50,55] because of either screened electrostatic interactions or short-range hydration forces. However, it is interesting to note that the decay lengths obtained from our experiments are extremely small, ranging from a few angstroms at low charge densities to tenths of angstroms at high charge densities. Such short decay lengths may reflect the monomer−monomer repulsion length scales of the polyelectrolyte chains, as they are much smaller than any electrostatic or hydration screening lengths. Compression of a phase through the application of osmotic stress eventually gives rise to phase transformations due to reductions in spontaneous curvature and the accompanying driving force for increased packing efficiency. In this context, it was assumed that the salt contribution to the osmotic pressure was negligible.

Coexistence Regions. As shown in Figures 2b and 3a,b, phase transitions from *Pm*3*n* cubic to hexagonal cylinders often proceeded through two-phase coexistence regions. Other groups have observed this sort of cubic−hexagonal coexistence for polyelectrolyte−surfactant complexes in which surfactant concentration was being increased.[21,22,38,56] The SAXS traces shown in Figure 4 illustrate how the hexagonal phase evolves from the cubic phase as osmotic pressure is increased in two different systems—the (100), (110), and (200) hcpc

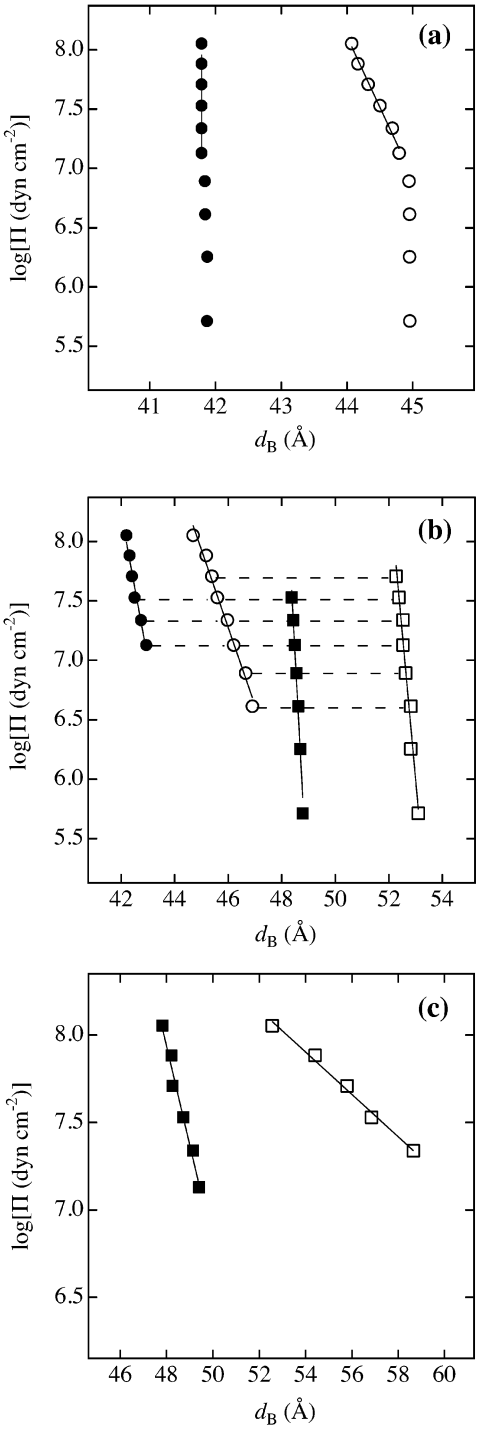

Figure 2. Phase diagrams of PAAm−CTA$^+$ complexes in 10 mM NaBr (filled symbols) and 100 mM NaBr (open symbols): (a) 100% charge, (b) 70% charge, and (c) 40% charge. Horizontal dashed lines indicate regions of coexistence between hcpc phases (●, ○) and *Pm*3*n* cubic phases (■, □). The points plotted represent the (100) hcpc diffraction signals and the (210) *Pm*3*n* cubic diffraction signals when those phases are present. The straight lines are exponential curve fits of the data whose slopes are plotted in Figure 6.

diffraction signals increase in intensity as osmotic pressure is increased.

In addition to inducing order−order transitions within well-structured complexes, the application of osmotic stress to a system possessing initially poor long-range order can promote the formation of a well-ordered phase. Figure 5 shows the evolution of a well-ordered *Pm*3*n*

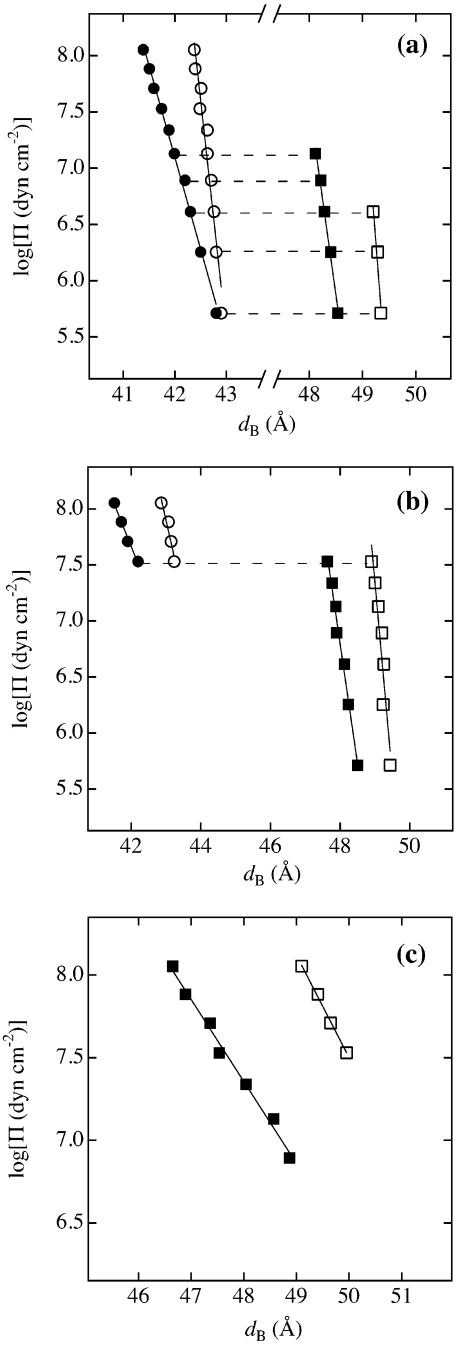

Figure 3. Phase diagrams of PAAm−CTA^+ complexes in 10 mM NaCl (filled symbols) and 100 mM NaCl (open symbols): (a) 100% charge, (b) 70% charge, and (c) 40% charge. Horizontal dashed lines indicate regions of coexistence between hcpc phases (●, ○) and *Pm*3*n* cubic phases (■, □). The points plotted represent the (100) hcpc diffraction signals and the (210) *Pm*3*n* cubic diffraction signals when those phases are present. The straight lines are exponential curve fits of the data whose slopes are plotted in Figure 6.

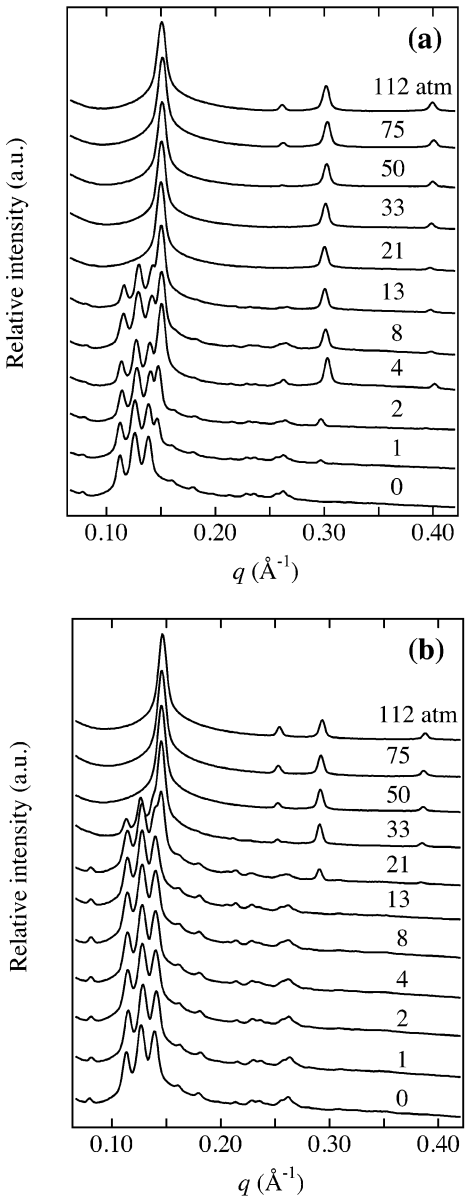

Figure 4. Angular-averaged scattering profiles for (a) 100% charge PAAm−CTA^+ complexes in 10 mM NaCl and (b) 70% charge PAAm−CTA^+ complexes in 100 mM NaBr, showing the evolution of the hcpc phase from the *Pm*3*n* phase with increasing osmotic pressure.

cubic phase from an indeterminate, poorly ordered structure in the 40% charge system as osmotic pressure was increased.

As mentioned earlier, the well-defined thermodynamic conditions under which osmotic stress experiments are carried out preclude the existence of two-phase regions—all chemical potentials are identical at equilibrium. However, it is quite possible that the systems which exhibit cubic−hexagonal coexistence regions have not yet reached their true equilibrium states. This would be a likely scenario if the two phases are energetically similar or if the kinetic barriers associated with the transition are sufficiently large. Such behavior is analogous to the topologically hindered structural transitions of liquid-crystalline lipid−water systems that have been studied as functions of hydrostatic pressure[57] and temperature.[58] A detailed analysis of the cubic−hexagonal coexistence regions in PAAm−CTA^+ complexes, including a discussion of the energetics of the cubic to hexagonal transition in these systems, is beyond the scope of this study and will be reported in a separate publication.

Charge Density Effects. At 10% polyelectrolyte charge content, no insoluble complex could be isolated after following the preparatory procedure described earlier. The lack of a solid precipitate at this low charge density is probably due to the fact that the entropy gain due to counterion release (upon binding to the surfactant) does not exceed the cost of restricting the configurational

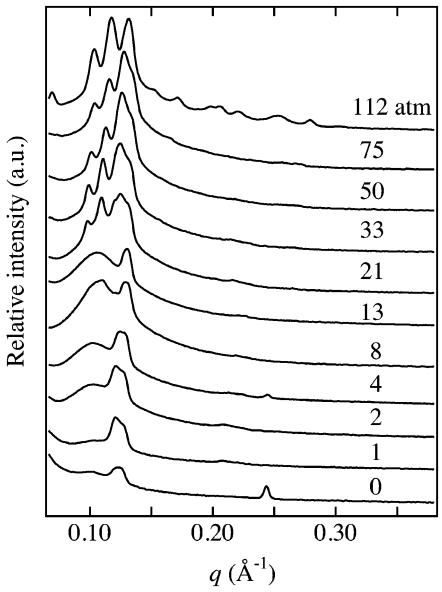

Figure 5. Angular-averaged scattering profiles for PAAm−CTA^+ complexes in 100 mM NaBr showing the evolution of a well-ordered *Pm*3*n* structure from an indeterminate, poorly ordered structure with increasing osmotic pressure.

Table 2. Dependence of PAAm−CTA^+ Unit Cell Sizes on Polyelectrolyte Charge Density in 100 mM NaBr

	a_{hcpc} (Å)		a_{Pm3n} (Å)	
Π (atm)	100%	70%	70%	40%
110	50.9	51.6		117.5
75	51.0	52.2		121.7
50	51.2	52.4	116.9	124.8
33	51.4	52.6	117.1	127.1
21	51.6	53.1	117.5	131.2

entropy of the polyelectrolyte by creating a structured complex. In fact, the distance between charged groups along the polyelectrolyte chain of approximately 30 Å exceeds the Bjerrum length of 7.1 Å, and therefore, according to the Manning condensation picture,[29] none of the counterions are condensed and accordingly no entropy can be gained by binding. Interestingly, at 40% charge density the distance between charges along the polyelectrolyte is approximately 7.5 Å (assuming a fully stretched chain), which suggests that there must exist additional driving forces for precipitation than just counterion release from the polyelectrolyte (see also Introduction). We still believe though that counterion release is the dominating driving force for complexation (for 100% and 70% charge density) as evidenced by the dependence of unit cell size on salt concentration discussed in the next section.

We found that by decreasing the polyelectrolyte charge density while holding other factors fixed tended to increase unit cell sizes, as shown in Table 2. Presumably, at low charge densities, more neutral monomers will be allowed to fill the spaces between surfactant moieties than at higher charge contents, thereby increasing the unit cell size.

These data also show that an increase in polymer charge density (while holding other conditions fixed) shifts the phase sequence toward more densely packed structures. For example, a cubic phase will be converted to a hexagonal phase as polymer charge density is increased, and Figure 2a−c reflects this increase in phase density with increasing charge content explicitly.

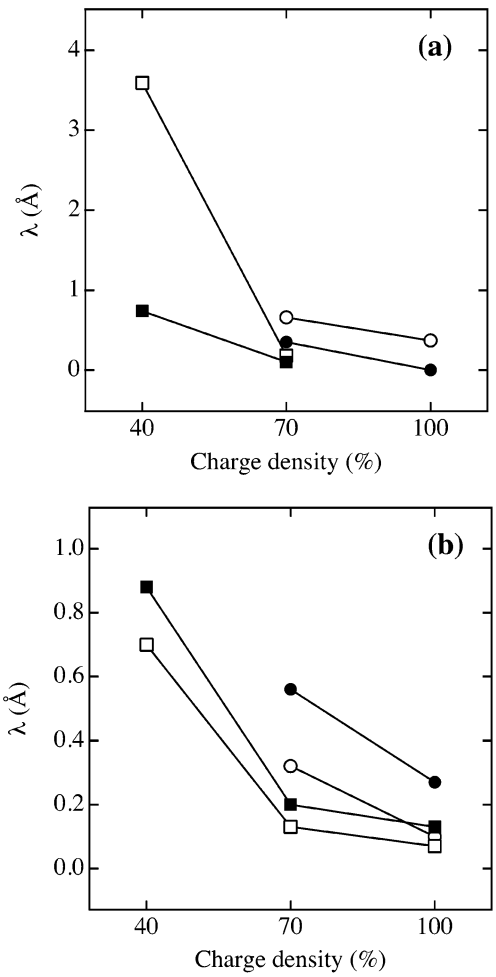

Figure 6. Exponential decay lengths of the hcpc (●, ○) and *Pm*3*n* cubic phases (■, □) from PAAm−CTA^+ complexes in (a) NaBr and (b) NaCl. Ionic strengths ranged from 10 mM (filled symbols) to 100 mM (open symbols).

As mentioned earlier, length scales of the exponential forces present between surfactant moieties are directly related to the decay lengths of the osmotic pressure vs distance curves obtained experimentally. Such decay lengths are also indicative of complex compressibilities—large decay lengths indicate a higher degree of compressibility compared to smaller decay lengths. As shown in Figure 6, decay lengths tended to decrease with increasing charge density. This again is an indication for the counterion release mechanism because the strength of association is directly related to the charge density of the polyelectrolyte.

Effects of Ionic Strength and Salt Type. In both salts, increasing the ionic strength while holding all other factors fixed brought about an increase of unit cell size within each observed phase —a clear indication of counterion release.[26−28] This is reasonable, considering that at higher bulk ionic strengths the entropic gain of the counterions upon adsorption of the polyelectrolyte chain will be reduced relative to lower ionic strengths.

Figure 6 shows that exponential decay lengths increased as bromide concentration was increased. This may be related to the well-known fact that bromide has a particularly strong affinity for the quaternary ammonium ion.[59,60] This driving force to bind with the surfactant headgroup may be so strong as to bring about the displacement of small sections of the polyelectrolyte chain that are bound to the surfactant as it competes

Table 3. Dependence of PAAm−CTA$^+$ Unit Cell Dimensions on Ionic Strength in NaBr at Π = 33 atm

charge density (%)	a_{hcpc} (Å)		a_{Pm3n} (Å)	
	10 mM	100 mM	10 mM	100 mM
100	48.3	51.4		
70	49.1	52.6	108.2	117.1
40			108.9	127.1

Table 4. Unit Cell Sizes for PAAm−CTA$^+$ in 1 M NaCl

charge density (%)	structure	Π_i (atm)	Π_f (atm)	a_i (Å)	a_f (Å)
100	hcpc	4	110	56.3	47.5
70	hcpc	4	110	56.3	49.1
70	*Pm*3*n*	33	110	102.2	99.8
40	hcpc	4	110	56.2	49.0

for the same binding sites. In this way, the presence of bromide ions would reduce the effective charge density of the surfactant. Therefore, as more bromide ions are introduced into the system, it should have the same effect as reducing the polymer charge density. This sort of exchange between polyacrylate and bromide ion has been previously reported by Ilekti et al.[17,39]

For the complexes equilibrated in chloride ion, it seems strange that higher ionic strengths should bring about smaller decay lengths, since Bragg spacings at fixed pressures tend to be larger at higher chloride concentration—again, one would expect that a higher polymer matrix density would translate into a higher compressibility. However, this is not what we observe, and the reason for this sort of behavior is unclear.

In a similar fashion, the presence of bromide ion favors the formation of higher density phases compared with the chloride ion; this is consistent with previously reported work.[38] For example, at 100% polyelectrolyte charge, hexagonal cylinders are observed at all osmotic pressures in both 10 and 100 mM bromide, whereas a combination of cubic and hexagonal phases is observed for the same system in chloride. However, when charge density is reduced below 100%, *Pm*3*n* phases are observed to coexist with the hcpc phase.

Phase Behavior in 1 M Salt. In 1 M NaBr, solid CTABr precipitated from each sample, and no discernible complex was observed. However, the presence of 1 M NaCl did not have such deleterious effects on the complexes, and osmotic pressure vs distance curves for complexes prepared under these conditions are shown in Figure 7. No insoluble complexes were observed in 1 M NaCl at osmotic pressures below 5 atm. At pressures greater than this, however, hexagonal cylindrical phases were observed as osmotic pressure was increased. In contrast to the results obtained in 10 and 100 mM salt, the curves obtained in 1 M salt are not smoothly exponential—the Bragg distance depends on osmotic pressure in a more complicated way. Also, the complexes are compressible over a considerably larger range under these conditions, as shown in Table 4. In addition, the osmotic pressure vs distance curves for each system can essentially be superimposed; the effect of charge density on unit cell dimensions is relatively insignificant in this case.

The degree of long-range order, as shown by SAXS, tended to decrease in 1 M salt. In most cases, fewer higher-order peaks were observed in this regime relative to the same systems at lower salt concentrations. Moreover, a coexistence region of hexagonal cylinders and *Pm*3*n* cubic structures was observed at high osmotic pressures in the 70% charge system. SAXS traces

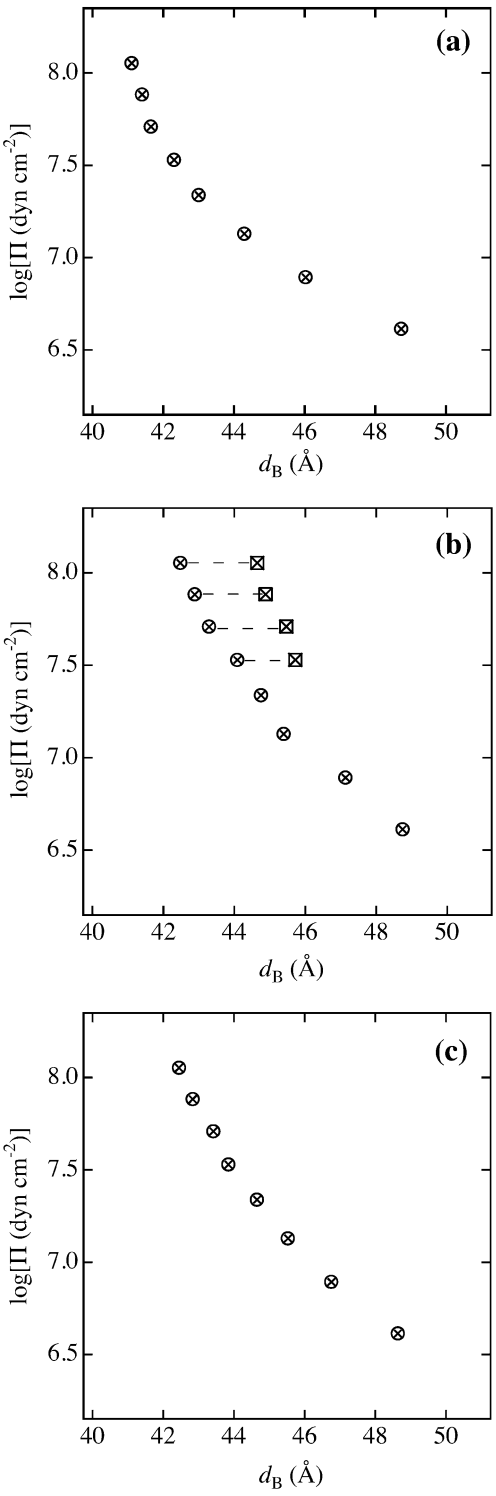

Figure 7. Phase diagrams of PAAm−CTA$^+$ complexes in 1 M NaCl: (a) 100% charge, (b) 70% charge, and (c) 40% charge. Horizontal dashed lines indicate regions of coexistence between hcpc phases (○) and *Pm*3*n* cubic phases (□). The points plotted represent the (100) hcpc diffraction signals and the (210) *Pm*3*n* cubic diffraction signals, when those phases were present.

obtained at each osmotic pressure for both the 100% and 70% charge systems are shown in Figure 8. It is currently unclear why coexistence is unique to the 70% charge system as well as why hexagonal cylinders dominate the phase diagram under these conditions. Considering these results, and the fact that CTABr precipitated from all samples in 1 M bromide, it is likely that the complexes become nonstoichiometric

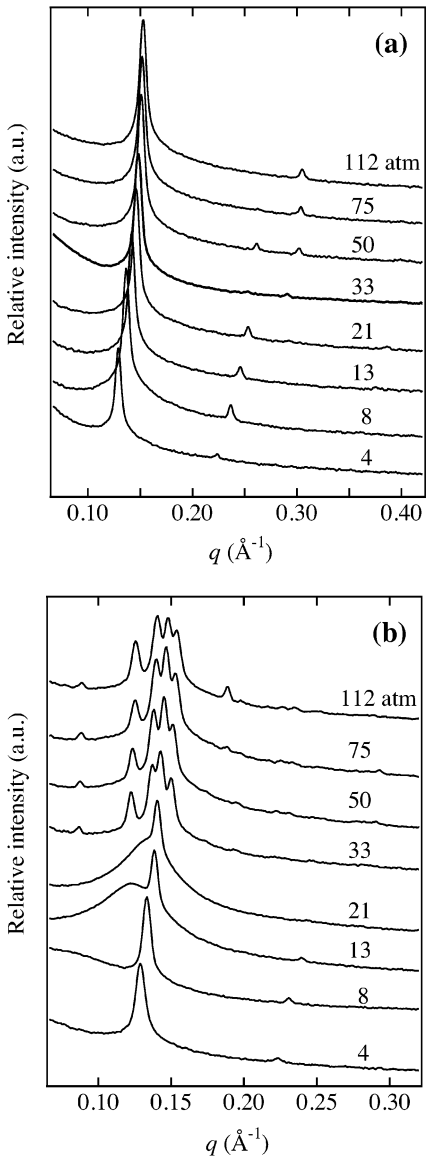

Figure 8. Angular-averaged scattering profiles for (a) 100% charge PAAm−CTA^+ complexes and (b) 70% charge PAAm−CTA^+ complexes under osmotic stress in 1 M NaCl. Traces are labeled with their corresponding osmotic pressure values.

at high salt concentrations. Other studies dealing with polyelectrolyte−surfactant complexes at high ionic strengths[61−64] have also postulated this departure from stoichiometry. Clearly, the trends observed for complexes in 10 and 100 mM salt cannot be extended to this high-salt, presumably nonstoichiometric regime.

Phase Behavior at Higher Pressures Using Salt Solution Vapor. As mentioned earlier, no salt was added to the complexes equilibrated against saturated salt solution vapor. As such, effects of ionic strength in this regime are not considered. Phase diagrams for these systems are shown in Figure 9. Coexistence regions of lamellar and hexagonal structures dominate the phase diagram under these conditions, and Bragg spacings were observed to decrease with increasing pressure, as expected. However, there is not enough resolution in this phase diagram to comment on the nature of the forces between assemblies or on the precise locations of the phase boundaries.

A pure lamellar phase was observed at 100% charge and 57% relative humidity, and in this case, Bragg

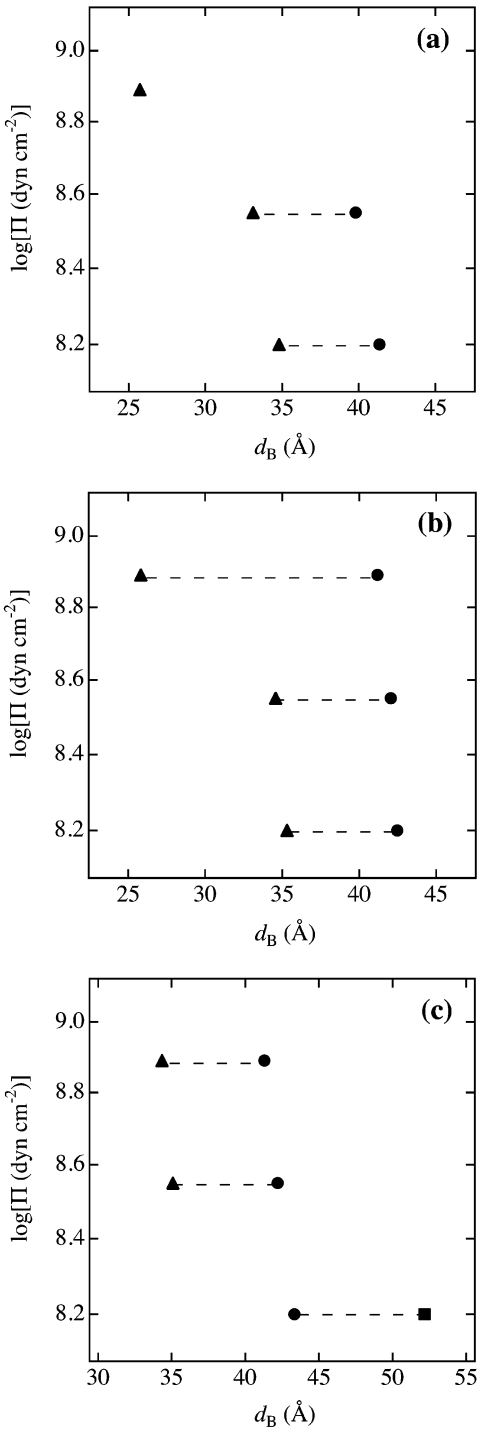

Figure 9. Phase diagrams of PAAm−CTA^+ complexes exposed to saturated salt vapor: (a) 100% charge, (b) 70% charge, and (c) 40% charge. Horizontal dashed lines connect regions of coexistence between hcpc phases (▲), *Pm*3*n* cubic phases (●), and lamellar phases (■), where applicable. The points plotted represent the (100) hcpc diffraction signals, the (210) *Pm*3*n* cubic diffraction signals, and the (100) lamellar diffractions signals when those phases were present.

spacings are indicative of the lamellar long period. SAXS traces obtained for each experiment are shown in Figure 10 and illustrate the structural evolution with increasing pressure. All charge densities were affected by increased pressure from salt vapor; structures that were not accessible with solution stress alone can be accessed with this method. For example, the densest phase that could be accessed for the 40% charge system was a well-

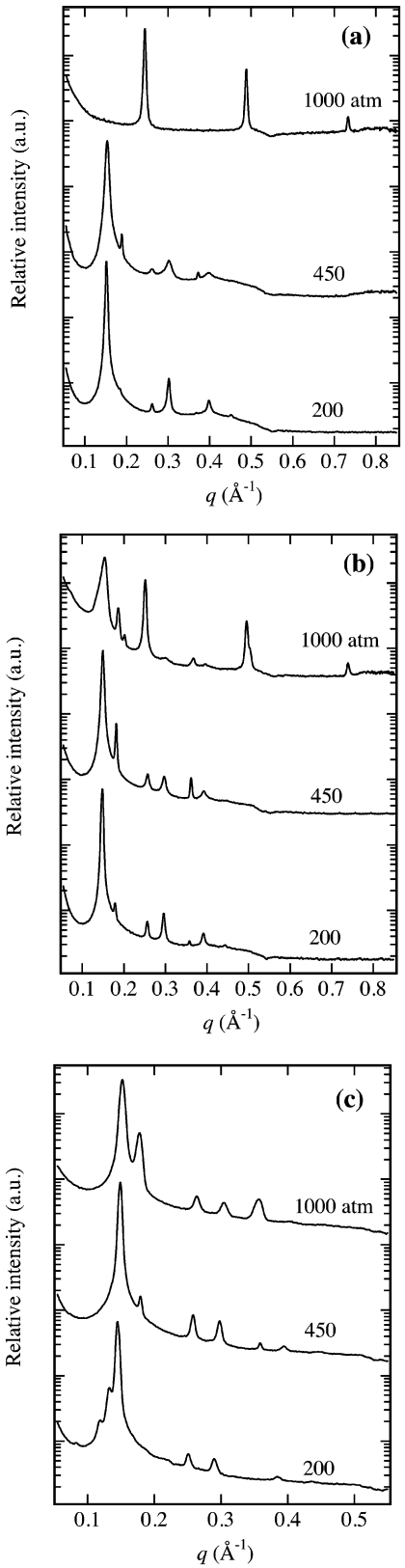

Figure 10. Angular-averaged scattering profiles for PAAm−CTA^+ complexes exposed to saturated salt vapor. Data are reported at relative humidities of 57% (NaBr), 77% (CH_3CO_2-Na), and 89% (KCl) with corresponding osmotic pressures listed: (a) 100% charge, (b) 70% charge, and (c) 40% charge.

ordered *Pm*3*n* phase, but both lamellar and hexagonal phases were observed for this system at the lower relative humidities available via saturated salt vapor.

Conclusions

Self-assembled PAAm−CTA^+ complexes exhibiting high degrees of nanoscopic order have been prepared, and comprehensive phase diagrams of these systems have been mapped as functions of polyelectrolyte charge density, ionic strength, salt type, and osmotic pressure, using a combination of solution osmotic stress and saturated salt vapor. A phase progression of *Pm*3*n* cubic ↔ hcpc ↔ lamellar was observed with decreasing complex water content, and the general trends we observed can be explained in terms of counterion release and the competition between packing constraints and spontaneous curvature. These factors, along with the occurrence of a *Pm*3*n* phase in our systems, help to distinguish polyelectrolyte−surfactant complexes from pure surfactant systems. The presence of coexistence regions between hcpc and *Pm*3*n* phases under certain conditions may be due to the energetic similarity of these two phases or due to kinetic barriers which do not allow for complete equilibration of the system on the laboratory time scale.

Acknowledgment. We gratefully acknowledge the National Science Foundation for supporting this work through the University of Massachusetts Amherst Materials Research Science and Engineering Center (DMR-0213695).

References and Notes

(1) Holm, C., Kékicheff, P., Podgornik, R., Eds.; *Electrostatic Effects in Soft Matter and Biophysics*; Kluwer Academic Publishers: Dordrecht, 2001.
(2) Darnell, J.; Lodish, H.; Baltimore, D. *Molecular Cell. Biology*, 2nd ed.; Scientific American Books: New York, 1990.
(3) Bloomfield, V. A. *Curr. Opin. Struct. Biol.* **1996**, *6*, 334−341.
(4) Strey, H. H.; Podgornik, R.; Rau, D. C.; Parsegian, V. A. *Curr. Opin. Struct. Biol.* **1998**, *8*, 309−313.
(5) Podgornik, R.; Strey, H. H.; Parsegian, V. A. *Curr. Opin. Colloid Interface Sci.* **1998**, *3*, 534−539.
(6) Camejo, G.; Fager, G.; Rosengren, B.; Hurtcamejo, E.; Bondjers, G. *J. Biol. Chem.* **1993**, *268*, 14131−14137.
(7) Camejo, G.; Lopez, A.; Lopez, F.; Quinones, J. *Atherosclerosis* **1985**, *55*, 93−105.
(8) Diamant, H.; Andelman, D. *Europhys. Lett.* **1999**, *48*, 170−176.
(9) Diamant, H.; Andelman, D. *Macromolecules* **2000**, *33*, 8050−8061.
(10) Hansson, P. *Langmuir* **2001**, *17*, 4167−4180.
(11) Wallin, T.; Linse, P. *Langmuir* **1998**, *14*, 2940−2949.
(12) Ober, C. K.; Wegner, G. *Adv. Mater.* **1997**, *9*, 17−31.
(13) Thalberg, K.; Lindman, B. *Langmuir* **1991**, *7*, 277−283.
(14) Thalberg, K.; Lindman, B.; Bergfeldt, K. *Langmuir* **1991**, *7*, 2893−2898.
(15) Goddard, E. D. *Colloids Surf.* **1986**, *19*, 301−329.
(16) Isogai, N.; Narita, T.; Chen, L.; Hirata, M.; Gong, J.; Osada, Y. *Colloids Surf. A* **1999**, *147*, 189−201.
(17) Ilekti, P.; Martin, T.; Cabane, B.; Piculell, L. *J. Phys. Chem. B* **1999**, *103*, 9831−9840.
(18) Antonietti, M.; Conrad, J.; Thünemann, A. *Macromolecules* **1994**, *27*, 6007−6011.
(19) Zhou, S.; Yeh, F.; Burger, C.; Chu, B. *J. Polym. Sci., Part B: Polym. Phys.* **1999**, *37*, 2165−2172.
(20) Zhou, S.; Yeh, F.; Burger, C.; Chu, B. *ACS Symp. Ser.* **2000**, *739*, 244−260.
(21) Kogej, K.; Theunissen, E.; Reynaers, H. *Langmuir* **2002**, *18*, 8799−8805.
(22) Kogej, K.; Evmenenko, G.; Theunissen, E.; Berghmans, H.; Reynaers, H. *Langmuir* **2001**, *17*, 3175−3184.
(23) Sokolov, E. L.; Yeh, F.; Khokhlov, A. R.; Grinberg, V. Y.; Chu, B. *J. Phys. Chem. B* **1998**, *102*, 7091−7098.
(24) Leonard, M. J.; Hong, H. M.; Easwar, N.; Strey, H. H. *Polymer* **2001**, *42*, 235−239.
(25) Dembo, A. T.; Yakunin, A. N.; Zaitsev, V. S.; Mironov, A. V.; Starodoubtsev, S. G.; Khokhlov, A. R.; Chu, B. *J. Polym. Sci., Part B: Polym. Phys.* **1996**, *34*, 2893−2898.

(26) Wagner, K.; Harries, D.; May, S.; Kahl, V.; Rädler, J. O.; Ben-Shaul, A. *Langmuir* **2000**, *16*, 303−306.
(27) Sens, P.; Joanny, J.-F. *Phys. Rev. Lett.* **2000**, *84*, 4862−4865.
(28) Joanny, J.-F.; Castelnovo, M.; Netz, R. *J. Phys.: Condens. Matter* **2000**, *12*, A1-A7.
(29) Manning, G. S. *Acc. Chem. Res.* **1979**, *12*, 443−449.
(30) Kosmella, S.; Kötz, J.; Shirahama, K.; Liu, J. *J. Phys. Chem. B* **1998**, *102*, 6459−6464.
(31) Li, Y.; Dubin, P. L.; Havel, H. A.; Edwards, S. L.; Dautzenberg, H. *Langmuir* **1995**, *11*, 2486−2492.
(32) Antonietti, M.; Wenzel, A. *Colloids Surf. A* **1998**, *135*, 141−147.
(33) Zhou, S.; Burger, C.; Yeh, F.; Chu, B. *Macromolecules* **1998**, *31*, 8157−8163.
(34) Zhou, S.; Hu, H.; Burger, C.; Chu, B. *Macromolecules* **2001**, *34*, 1772−1778.
(35) Sokolov, E. L.; Yeh, F.; Khokhlov, A. R.; Chu, B. *Langmuir* **1996**, *12*, 6229−6234.
(36) Merta, J.; Torkkeli, M.; Ikonen, T.; Serimaa, R.; Stenius, P. *Macromolecules* **2001**, *34*, 2937−2946.
(37) Mironov, A. V.; Starodoubtsev, S. G.; Khokhlov, A. R.; Dembo, A. T.; Yakunin, A. N. *Colloids Surf. A* **1999**, *147*, 213−220.
(38) Svensson, A.; Piculell, L.; Cabane, B.; Ilekti, P. *J. Phys. Chem. B* **2002**, *106*, 1013−1018.
(39) Ilekti, P.; Piculell, L.; Tournilhac, F.; Cabane, B. *J. Phys. Chem. B* **1998**, *102*, 344−351.
(40) Michel, B. E. *Plant Physiol.* **1983**, *72*, 66.
(41) Michel, B. E.; Kaufmann, R. *Plant Physiol.* **1973**, *51*, 914.
(42) Stanley, C. B.; Strey, H. H. *Macromolecules* **2003**, *36*, 6888−6893.
(43) Lide, D. R., Ed.; *CRC Handbook of Chemistry and Physics*, 73rd ed.; CRC Press: Boca Raton, FL, 1993.
(44) Parsegian, V. A.; Fuller, N. L.; Rand, R. P. *Proc. Natl. Acad. Sci. U.S.A.* **1979**, *76*, 2750−2754.
(45) Lis, L. J.; McAlister, M.; Fuller, N. L.; Rand, R. P.; Parsegian, V. A. *Biophys. J.* **1982**, *37*, 657−665.
(46) Leikin, S.; Rau, D. C.; Parsegian, V. A. *Phys. Rev. A* **1991**, *44*, 5272−5278.
(47) Leikin, S.; Rau, D. C.; Parsegian, V. A. *Proc. Natl. Acad. Sci. U.S.A.* **1994**, *91*, 276−280.
(48) Rau, D. C.; Parsegian, V. A. *Science* **1990**, *249*, 1278−1281.
(49) Bonnet-Gonnet, C.; Leikin, S.; Chi, S.; Rau, D. C.; Parsegian, V. A. *J. Phys. Chem. B* **2001**, *105*, 1877−1886.
(50) Strey, H. H.; Parsegian, V. A.; Podgornik, R. *Phys. Rev. Lett.* **1997**, *78*, 895−898.
(51) Kékicheff, P.; Grabielle-Madelmont, C.; Ollivon, M. *J. Colloid Interface Sci.* **1989**, *131*, 112−132.
(52) Auvray, X.; Petipas, C.; Anthore, R.; Rico, I.; Lattes, A. *J. Phys. Chem.* **1989**, *93*, 7458−7464.
(53) Fontell, K. *Colloid Polym. Sci.* **1990**, *268*, 264−285.
(54) Ziherl, P.; Kamien, R. D. *Phys. Rev. Lett.* **2000**, *85*, 3528−3531.
(55) Parsegian, V. A.; Rand, R. P.; Fuller, N. L.; Rau, D. C. In *Methods in Enzymology*; Packer, L., Ed.; Academic Press: New York, 1986; Vol. 127, pp 400−416.
(56) Hansson, P.; Schneider, S.; Lindman, B. *J. Phys. Chem. B* **2002**, *106*, 9777−9793.
(57) So, P. T. C.; Gruner, S. M.; Erramilli, S. *Phys. Rev. Lett.* **1993**, *70*, 3455−3458.
(58) Toombes, G. E. S.; Finnefrock, A. C.; Tate, M. W.; Gruner, S. M. *Biophys. J.* **2002**, *82*, 2504−2510.
(59) Ozeki, S.; Ikeda, S. *J. Colloid Interface Sci.* **1982**, *87*, 424−435.
(60) Imae, T.; Kamiya, R.; Ikeda, S. *J. Colloid Interface Sci.* **1985**, *108*, 215−225.
(61) Thalberg, K.; Lindman, B. *Colloids Surf. A* **1993**, *76*, 283−288.
(62) Mironov, A. V.; Starodoubtsev, S. G.; Khokhlov, A. R.; Dembo, A. T.; Yakunin, A. N. *Macromolecules* **1998**, *31*, 7698−7705.
(63) Thalberg, K.; Lindman, B.; Karlström, G. *J. Phys. Chem.* **1991**, *95*, 6004−6011.
(64) Skepö, M.; Linse, P. *Phys. Rev. E* **2002**, *66*, 051807.

MA034352C